F. D. Chitty, C. J. Freeman, and D. B. Garber, "Joint Design Optimization for Accelerated Construction of Slab Beam Bridges," *Journal of Bridge Engineering*, vol. 25, no. 7. p. 04020029-14, 2020

Joint Design Optimization for Accelerated Construction of Slab Beam Bridges

F. D. Chitty[1], C. J. Freeman[2], and D. B. Garber[3]

[1] Graduate Research Assistant, Dept. of Civil and Environmental Engineering, Florida International University, 10555 West Flagler Street, Miami, FL 33174, (corresponding author). Email: fchit001@fiu.edu

[2] Structures Research Engineer, Structures Research Center, Florida Department of Transportation, 2007 E. Paul Dirac Dr. Tallahassee, FL 32310. Email: christina.freeman@dot.state.fl.us

[3] Assistant Professor, Dept. of Civil and Environmental Engineering, Florida International University, 10555 West Flagler Street, Miami, FL 33174. Email: dgarber@fiu.edu

ABSTRACT

The Florida Slab Beam (FSB) has been developed by the Florida Department of Transportation (FDOT) to be used for short-span bridges (less than about 19.8 m [65 ft.] long). The FSB system consists of shallow precast, prestressed concrete inverted-tee beams that are placed adjacent to each other and then involve reinforcement and concrete being placed in the inner joints and deck all in one single cast. Ultra-high-performance concrete (UHPC) is becoming more widely used in bridge construction applications due to its remarkable structural performance. Many departments of transportation have tested and deployed the use of UHPC in bridges around the US. Most of these applications have been to connect precast members (e.g. slabs to beams and slabs, adjacent beams, caps to columns, etc.). A modified FSB design is desired to eliminate the cast-in-place (CIP) deck and allow for UHPC to be used in the joint region, which will allow for accelerated

F. D. Chitty, C. J. Freeman, and D. B. Garber, “Joint Design Optimization for Accelerated Construction of Slab Beam Bridges,” *Journal of Bridge Engineering*, vol. 25, no. 7. p. 04020029-14, 2020

construction and decrease the impact of construction on traffic. Different joint details and cross-section geometries were analyzed and experimentally evaluated to determine feasible joint details with UHPC for slab beam bridges used in accelerated construction. Results from numerical modeling, strength, and fatigue experimental testing of the transverse joint performance of four different UHPC joints in two different depth slab beam bridges are presented. The straight-side and shear-key UHPC joint details were found to behave similar to or better than the current FSB joint detail.

CE Database Keywords:

Ultra-high performance concrete, accelerated bridge construction, prefabricated elements and systems, non-linear finite element analysis, slab beam bridge

INTRODUCTION

There are over 600,000 bridges in the US with about 40 percent of them at least 50 years old and about nine percent of them being structurally deficient (American Society of Civil Engineers (ASCE), 2017). In Florida, the majority of the structurally deficient or functionally obsolete bridges are short-span bridges, including slab beam systems with deficient load transfer capacity due to strength decay in their joints; approximately 90 percent of these bridges are less than 18 m (60 ft.) long (Nolan, Freeman, Kelley, & Rossini, 2018). There has been a need to develop solutions for rapidly replacing, repairing or retrofitting these structures while minimizing the impact to traffic during construction. Accelerated bridge construction (ABC) techniques, specifically prefabricated bridge elements and systems (PBES), can provide such a solution. Slab beam superstructures, one type of prefabricated element, can be used with ultra-high performance concrete (UHPC) to create a resilient superstructure system that can offer accelerated construction with enhanced serviceability performance. The development of a joint detail for such a slab beam system that enhances load transfer capacity through numerical modeling and experimental testing of joints in flexure is summarized in this paper.

Slab Beam Superstructures

Slab beams have been used in bridge superstructure construction since prestressing began in the United States in the 1950s. Slab beam superstructures are characterized by having shallow depth, prestressed, precast concrete, and are placed side-by-side with a concrete joint cast in between them. Due to their shallow depths, the beam section is typically suitable for bridge spans less than 22.9 m (75 ft.) in length. Texas (Texas Department of Transportation (TxDOT), 2018), Minnesota (Federal Highway Administration (FHWA), 2015), Virginia (Menkulasi, Mercer, Wollmann, & Cousins, 2012), and Florida departments of transportation have used different slab beam configurations with different longitudinal joint and transverse tie mechanisms to ensure appropriate load transfer between adjacent members. The Florida Department of Transportation (FDOT) bridge inventory has developed six iterations of slab beam bridges that have been built since the 1950s (Nolan et al., 2018). The first of these slab beam bridges was the prestressed rectangular slab unit, shown in Fig. 1 (a). This system did not have a cast-in-place (CIP) concrete deck and was connected through a longitudinal, 254 mm (10 in.) wide, concrete closure pour. The width of the joint was dependent on the required development length of the transverse steel projecting in the closure pour. In 1958, the system was modified to enhance its capacity by adding a 102-mm (4-in.) CIP reinforced concrete deck that was cast with the joint as shown in Fig. 1 (b). The joint was modified by extending the bottom concrete ledges such that forming underneath the superstructure was not required and transverse post-tensioned tie bars in sleeves were used as the transverse joint reinforcement. Later in the 1950s, a lighter version of the slab unit called Sonovoid (voided slab) began to be used, shown in Fig. 1 (c). Sonovoids have a reduced weight due to cylindrical voids running along the length of the beam and an asphalt layer in place of the 102-mm (4-in.) thick CIP deck; the asphalt overlay was used to accommodate differential camber between adjacent beams. The overall joint geometry was decreased to small shear keys filled with grout. The same transverse post-tensioned tie bar detail was used to provide for the force transfer between adjacent beams. These cross-sections developed by FDOT regional offices were used for the next few decades. The next major development in the FDOT slab beam systems was the Prestressed Slab Unit (PSU), shown in Fig. 1 (d), which first appeared in 2008 and was standardized in 2009. The PSU was simpler to construct in the field as it eliminated the need for transverse tie bars. The load transfer between adjacent members relied on a grouted shear key and a 153-mm (6-in.) thick CIP reinforced concrete deck that acted in composite action with the slab beams.

There have been some issues observed with existing slab beam systems in Florida (FDOT, 2013; Nolan et al., 2018) shown in Fig. 1 (a) – (d). The transverse capacity of the joint has decayed rapidly during service loading in some deployed bridges, indicated by longitudinal cracking at the joints along the length of the beams. This behavior would suggest that the slab beam superstructure system is not behaving as a composite unit, but rather load is being primarily carried by the beam on which it is directly applied.

Poor performance of these systems led FDOT to the development of an alternate system in 2005, the Florida Slab Beam (FSB), shown in Fig. 1 (e). The FSB was developed for use on low volume, short-span bridges (less than about 19.8 m [65 ft.] long). It consists of shallow precast, prestressed concrete inverted-tee beams that are placed side by side, allowing the bottom lip to serve as a bottom form for the CIP joint and deck. A steel reinforcement cage is placed in the joint region with an additional steel reinforcement mat for the top deck. A monolithic concrete joint and slab are cast after all the reinforcement is placed.

F. D. Chitty, C. J. Freeman, and D. B. Garber, "Joint Design Optimization for Accelerated Construction of Slab Beam Bridges," *Journal of Bridge Engineering*, vol. 25, no. 7. p. 04020029-14, 2020

The section shares some characteristics with the Precast Composite Slab Span System (PCSSS) developed by Minnesota in 2005 (Bell, French, & Shield, 2006; French et al., 2011; Smith, Eriksson, Shield, & French, 2008), shown in Fig. 1 (f), which was the first shallow inverted-T prestressed concrete system with straight web sides and bottom ledges that served as stay-in-place formwork. The main difference between the FSB and the PCSSS system is that the PCSSS has projecting rebar hooks that extend transversely through the joint creating a lapped splice, while the projecting rebar hooks in the FSB do not extend beyond the edge of the bottom lip. The detail in the FSB was intended to improve constructability by eliminating the potential of projecting rebars from adjacent members interfering with each other.

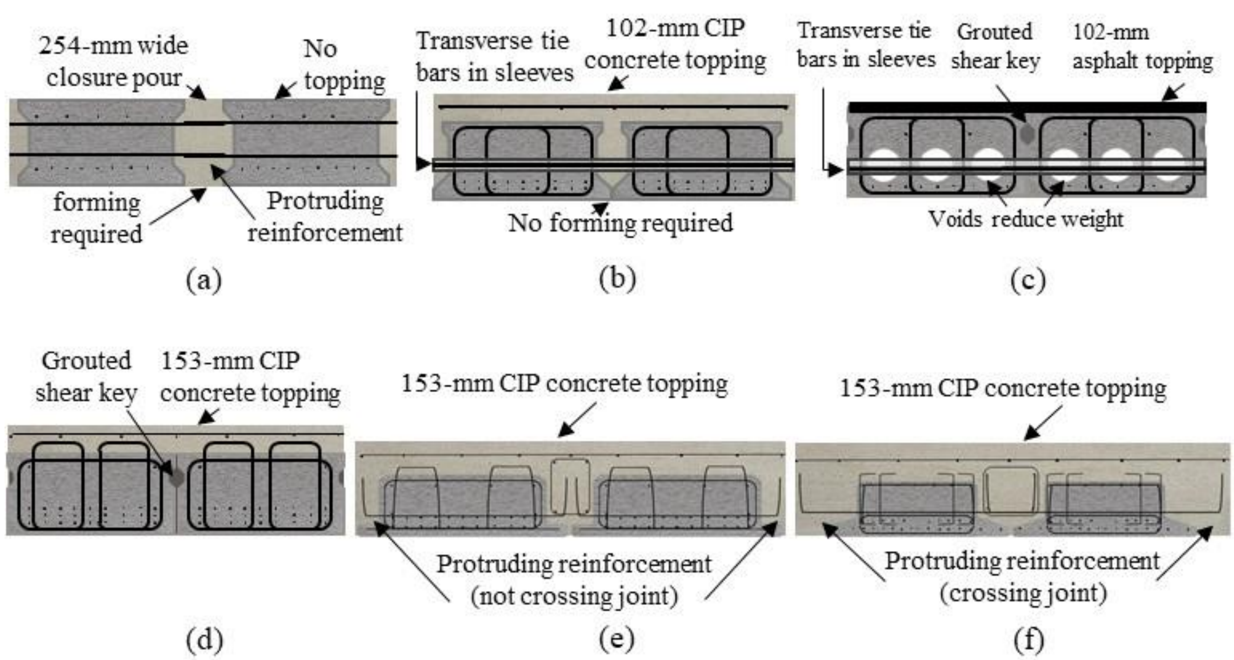

Fig. 1: *Slab beam system evolution in Florida: (a) prestressed rectangular slab unit (1955), (b) prestressed keyed slab unit (1958), (c) prestressed voided slab units – Sonovoid (1958), (d) prestressed slab unit – PSU (2008), (e) Florida Slab Beam – FSB (2015), based on* **(***Goldsberry***,** *2015), and (f) precast composite slab span system – PCSS (2005).*

After the PCSSS development, MnDOT implemented the system in two pilot bridge projects with one of the bridges instrumented and monitored to investigate the in-service performance and possible reflective cracks on the CIP deck (Smith et al., 2008). It was found that cracking initiated in CIP deck regions immediately above the vertical sides of the beam webs over the ledged joints, and the researchers determined that these cracks resulted from restrained concrete shrinkage and environmental effects rather than traffic loads (French et al., 2011; Smith et al., 2008). Ten additional bridges were constructed between 2005 and 2011, giving a total of 12 bridges constructed in Minnesota with a version of the PCSSS system. Five of these bridges were inspected in 2011 to determine their performance (Halverson, French, & Shield, 2012). Halverson et al. (2012) found there to be extensive cracking and efflorescence located on the bottom of the superstructure near joints in the inspected bridges. An optimized inverted T-beam was later proposed by researchers from Virginia with revised web section that included tapered sides. This solution was shown to decrease stress concentrations that could occur in abrupt geometry changes in the slab beam web (Menkulasi et al., 2012; Menkulasi, Cousins, & Wollmann, 2018), but researchers still found that stresses from temperature and time effects were still significant (Menkulasi et al., 2018).

Research Motivation, Objective, and Significance

The research discussed in this paper had two primary motivations: (1) the poor performance of previously used slab beam systems for short-span bridges evidenced by reflective cracking along the joint line in in-service bridges and (2) the desire to create a short-span bridge solution for accelerated construction. The primary objective of the research discussed in this paper was to develop a cross section for short-span bridges (less than 22.9 m [75 ft.] in length) and a joint design utilizing UHPC with satisfactory strength and fatigue performance, which allows for accelerated construction of the superstructure. UHPC was selected as the joint material for this research as it has been previously used in accelerated bridge construction applications to connect other precast members (e.g. full-depth precast deck panels, adjacent box beams). The research discussed in this paper is significant as it addresses the future construction of short-span bridges, which make up the vast majority of structurally deficient and functionally obsolete bridges.

Previously Investigated Joint Details with UHPC

Ultra-High-Performance Concrete (UHPC) is becoming more widely used due to its high compressive and tensile strength, improved long-term durability, low permeability, and high flowability. Also, UHPC has been used for constructing prefabricated bridge elements and overlays, but its primary application to date has been for the joints between prefabricated elements (Russell & Graybeal, 2013). The high tensile strength of UHPC decreases the required joint size and improves the joint durability between prefabricated elements; UHPC has been shown to provide a stronger connection than the prefabricated members themselves (Graybeal, 2010).

There have been several research efforts that have investigated UHPC joints between full-depth precast concrete deck panels (Aaleti & Sritharan, 2014; Graybeal, 2014b) and adjacent box beams (Yuan, Graybeal, & Zmetra, 2018). A study conducted by Aaleti and Sritharan (Aaleti & Sritharan, 2014) determined the four most popular joint geometries used in panel-to-panel connections with different steel rebar configurations: lap spliced bars, headed bars, non-contact lap spliced bars, and hooked bars. A UHPC joint geometry with non-contact, lap spliced transverse rebar was later developed to connect adjacent box bridge superstructures (Yuan et al., 2018); the details of this joint were based on previously discussed joint geometries.

Guidelines for UHPC field-cast joint construction were developed based on the extensive research conducted by the Federal Highway Administration (FHWA) (Graybeal, 2014a). These guidelines were developed based on findings from the previously mentioned research on joint connections, additional reinforcement pull out and development testing (Yuan & Graybeal, 2014), and UHPC material testing (Haber, De la Varga, Graybeal, Nakashoji, & El-Helou, 2018).

DEVELOPMENT OF UHPC JOINT GEOMETRY AND REINFORCEMENT DETAIL

The design embedment lengths, cover, lap splice length, and spacing between non-contact lap spliced bars in UHPC were chosen as recommended by Graybeal (Graybeal, 2014a) as a starting point. The recommended and provided values for the #16 (#5) joint reinforcement (d_b = 15.9 mm [0.625 in.]) are shown in Table 1; the joint regions proposed for testing use #16 (#5) rebar as the primary joint reinforcement. These design recommendations are valid for a UHPC mix with 2-percent (by volume) steel fiber reinforcement and a compressive strength of at least 96.46 MPa (14 ksi). This value allows for accelerated construction applications, as a typical UHPC mix can reach above 96.46 MPa (14 ksi) within the first few days after casting (Graybeal, 2006).

Table 1. *Design values for UHPC connections (based on (Graybeal, 2014a))*

Parameter	Formula	Value	Provided
Embedment Length	$l_d = 8d_b$	$8 * 15.9$ mm $= 127.2$ mm	127.2 mm or 161.9 mm
Cover	$\geq 3d_b$	$3 * 15.9$ mm $= 47.7$ mm	47.6 mm
Lap splice length	$l_s = 0.75l_d$	$0.75 * 127.2" = 95.4$ mm	101.6 mm or 133.3 mm
Max. clear spacing	l_s	95.2 mm	60.3 mm

Note: l_d = *embedment length;* l_s = *lap splice length; 1 in. = 25.4 mm*

Two categories of joint geometries were developed for investigation in this project: (1) straight joint sides with no shear key and (2) traditional shear key shape. The width of the joints with straight sides and no shear key was based on the required embedment length and splice length of the joint reinforcement. As UHPC allows for a shorter embedment and development lengths, only a 153-mm (6-in.) wide joint was required, resulting in two joint geometries called FDOT 1 (F1) and FDOT 2 (F2), as shown in Fig. 2 (a) and (b). A bottom lip was still provided in these joints to allow for the joint to be constructed without bottom forming of the joint. Two different thickness bottom lips were provided: a 102-mm (4-in.) lip with reinforcement extending into it in joint F1, and a 51-mm (2-in.) lip without reinforcement extending into the lip in joint F2, shown in Fig. 2 (a) and (b), respectively. The thinner bottom lip dimension allowed for the joint reinforcement to be moved further down in the section but did not allow for reinforcement to be extended into the lip.

One traditional shear key detail was chosen to allow for a larger embedment length of the joint reinforcement while keeping a similar joint area. This detail was based on a previously recommended detail for the connection between adjacent box beams (Graybeal, 2014a; Yuan et al., 2018), and it is called Alternate 1 (A1) as shown in Fig. 2 (c). The splice length of the joint reinforcement was the same as joint F1 and F2 previously described. The depth of the joint reinforcement in joint A1 (162 mm [6.4 in.]) was larger than that of joint F1 (158 mm [6.2 in.]). A second shear key detail, shown in Fig. 2 (d) and called Alternate 2 (A2), was developed to: (1) lower the height of the joint reinforcement, (2) increase the splice length of the reinforcement, and (3) strengthen the top flange portion of the joint.

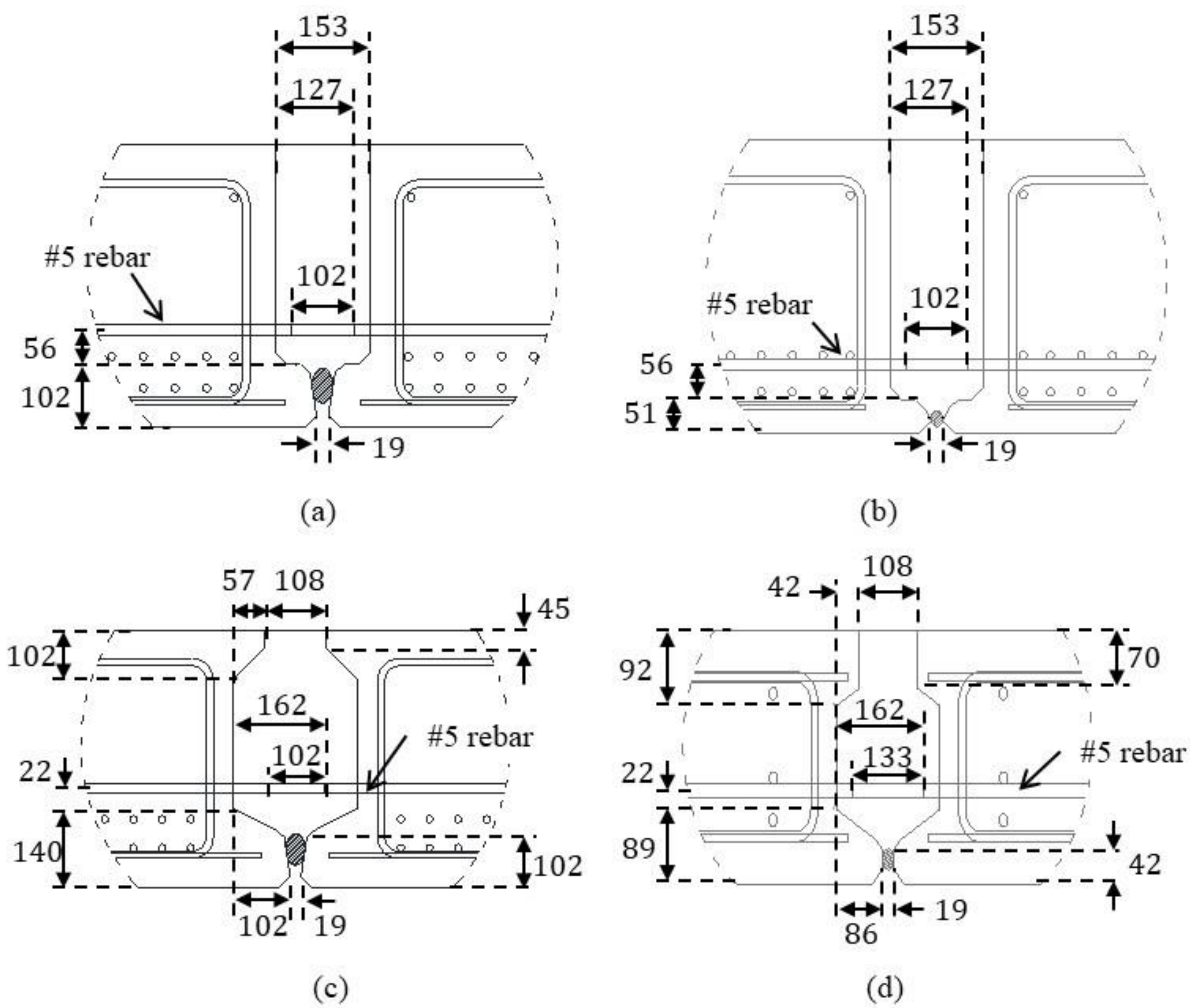

Fig. 2: *Details for joint: (a) FDOT 1 (F1), (b) FDOT 2 (F2), (c) Alternate 1 (A1), and (d) Alternate 2 (A2). (units: mm, 1 mm = 0.0394 in)*

The performance of the proposed UHPC joint specimens was compared to the performance of a control specimen, called FSB, which had a joint designed using the original FSB construction detail (FDOT, 2016b). This detail requires #16 (#5) hooked joint reinforcement with a bend diameter of 64 mm (2.5 in.) extending 127 mm (5 in.) from the precast beams with a height measured from the base of the member of 165 mm (6.5 in.), as shown in Fig. 1 (e). The reinforcement installed in the field includes hooped bars in the joint, longitudinal joint reinforcement along the length of the beam, and deck reinforcement all of which are #16 (#5) bars. The joint and CIP deck are then cast at the same time.

These joint details were evaluated through the following numerical and experimental investigations using 305-mm (12-in.) and 457-mm (18-in.) deep specimens with reinforcement details similar to those recommended by the original FSB construction guidance (FDOT, 2016b).

NUMERICAL INVESTIGATION

Finite element analysis (FEA) was first used to determine the failure mechanism of the proposed joint geometries. FEA served to initially evaluate the performance of the joints and to determine the geometry of the specimens (length, width, and depth) to ensure a flexural failure mechanism with expected failure loads within the testing frame capabilities.

Numerical Methods

The response of all the laboratory specimens were first estimated using a commercial non-linear FEA package named ATENA® specially designed for modeling reinforced concrete elements in the elastic, post-cracking, and ultimate capacity ranges. The software uses the Fracture-Plastic Constitutive Model: tensile (fracturing) and compressive (plastic) behavior (V. Cervenka, Jendele, & Cervenka, 2016), which is suitable to simulate concrete cracking, crushing under high confinement, and crack closure due to crushing in other material directions.

Specimen Geometry

Numerical models were developed for eight joint geometries to be tested in two groups: (1) 457-mm (18-in.) deep beams (Control FSB, F1, F2, and A1), and (2) 305-mm (12-in.) deep beams (F1, F2, A1, and A2), as shown in Fig. 3. These joint specimens consisted of two beams with the same joint geometry placed side by side and loaded to study the transverse flexural capacity of the joints. There are three main slab-beam depths in the current FSB Specifications (FDOT, 2016b). The control FSB specimen was designed using a 305-mm (12-in.) deep standard FSB section with a 1,520-mm (60-in.) wide (FSB 12x60) and a 152-mm (6-in.) deep CIP deck, giving an overall thickness of 457 mm (18 in.). The smallest and largest slab beam depths in the current FSB Specification (305 mm and 457 mm [12 in. and 18 in.]) were chosen for the investigation of the other UHPC joint specimens without CIP decks.

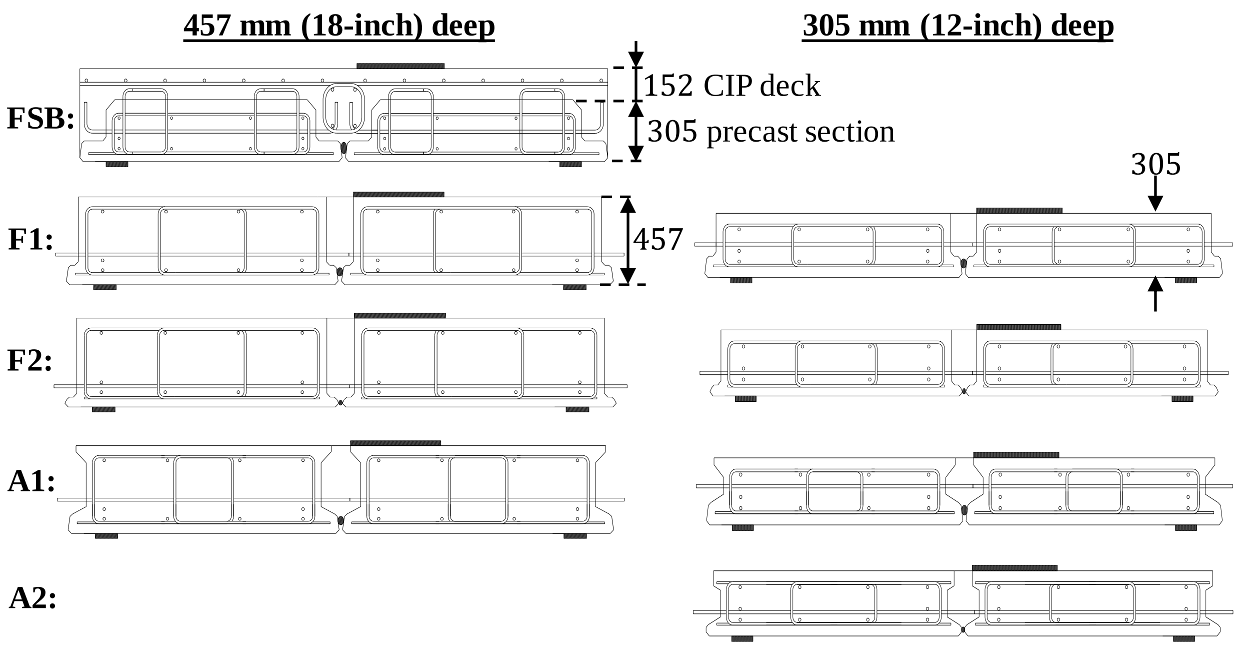

Fig. 3: *Specimen details for analytical and experimental program. (units: mm, 1 mm =0.0394 in)*

The FSB control served as a comparison for the 457-mm (18-in.) deep UHPC joint specimens. The overall thickness of the section is designated as the first number in the specimen name (e.g., 12F1 is a 12-inch thick specimen with joint F1).

Ten total 15-mm (0.6-in.) diameter prestressing strands were located parallel to the joint in the beam section. Four strands were spread out across the top of the section, four strands at the bottom of the section and two strands in the outside of the section 51 mm (2 in.) above the bottom row of strands, as shown in Fig. 3.

F. D. Chitty, C. J. Freeman, and D. B. Garber, "Joint Design Optimization for Accelerated Construction of Slab Beam Bridges," *Journal of Bridge Engineering*, vol. 25, no. 7. p. 04020029-14, 2020

Meshing and Material Models

The mesh of all the models were generated automatically using the default mesh size (102 mm [4 in.]) per element with a tetrahedra geometry. The material properties used for modeling the concrete, UHPC, and steel reinforcement in the sections are summarized in Table 2. The FSB section and conventional joint concretes were modeled using a conventional concrete model (CC3DNonLinCementitious2) with the described ultimate and compressive tensile stresses. The UHPC was also modeled using CC3DNonLinCementitious2, but with an increased compressive strength (f'_c), tensile strength (f_t), modulus of elasticity (E) and fracture energy (G_F), as shown in Table 2. The CC3DNonLinCementitious2 material consists of two constitutive models for fracture (tension) and plastic (compression) behaviors combined through a simultaneous algorithm solution (J. Cervenka & Papanikolaou, 2008). The crack initiation in the fracture model is computed using the Rankine failure criterion, which is described by a pyramid region formed by three stress planes in a stress space, or Rankine failure surface. A crack is formed when a maximum principal tensile stress (in any of the main three stress directions delimitated by the failure surface at any finite element) exceeds the tensile strength (f_t) of concrete (J. Cervenka & Papanikolaou, 2008). The crack opening is then determined by the crack band size and the fracture strain as suggested by Hordijk (Hordijk, 1991).

Table 2: *Summary of concrete and steel material models used*

Material	Base Material Prototype	f_y (MPa)	f'_c (MPa)	f_t (MPa)	E (GPa)	G_F (kN/m)
Beams*	CC3DNonLinCementitious2	--	58.6	3.8	30.0	0.080
Conventional Joint	CC3DNonLinCementitious2	--	27.6	2.2	30.0	0.050
UHPC Joint	CC3DNonLinCementitious2	--	126.2	5.5	42.7	0.125
Steel Reinforcement	CCReinforcement	413.7	--	--	199.9	--

Note*: f_y = yielding strength; f'_c = concrete compressive strength at 28 days; f_t = concrete tensile strength at 28 days; E = modulus of elasticity; *same material for all beams: Control FSB and specimens with modified joint geometry; 1 ksi = 6.9 MPa; 1 kip = 4.4 kN; 1 in. = 0.025 m.*

All the steel rebar in the models were specified as typical Grade 60 reinforcement without steel hardening. The longitudinal prestressing strands were modeled as inactive strands (without active prestressing force) as the models were used to assess the transverse behavior of the section and the joint strength.

The interface was modeled as a perfect bond between the UHPC and precast section, which was assumed because previous testing has shown that UHPC has a good bond to conventional concrete with proper aggregate exposure finish with at least 6-mm (0.25-in.) amplitude. Hence, the need for proper surface preparation for bond in joint specimens (Graybeal, 2014a).

Transverse Joint Capacity

The transverse joint capacity between two adjacent members was investigated through these numerical analyses using a similar joint testing protocol conducted by Graybeal (Graybeal, 2010). The boundary conditions, loading condition, and overall specimen geometry (for 1,422-mm [56-in.] long specimens) are shown in Fig. 4 (a) and (b). Two beam segments with a short length (1,422 mm and 2,845 mm [56 in. and 112 in.]) were placed side by side with a UHPC joint connecting them (or CIP deck and joint for the FSB control specimen). The supports were located toward the outside of the beams running parallel to the joint; note that this is perpendicular to the orientation of the bearings in a bridge in the field as this test measures the transverse response at bridge mid-span between two beams. The load was then placed on the center edge of the joint region (aligning the outer wheel patch border to the joint boundary line) to test both the shear transfer and flexure capacity of the joint. The load is applied through a load plate the size of an HS-20 wheel patch

(508 mm by 254 mm [20 in. by 10 in.]), as shown in Fig. 4 (b) based on the AASHTO LRFD Bridge Design Specifications (American Association of State Highway and Transportation Officials) (AASHTO, 2014) oriented in the direction of traffic parallel to the joint. Joints were tested using these support and load conditions for specimens with 1,422-mm and 2,845-mm (56-in. and 112-in.) lengths to determine the ultimate strength of the joint, joint ductility through the load-deflection response (based on deformation after non-linear stage), and failure mechanism determined by the crack pattern at failure. A sample crack pattern and load-deflection response are shown in Fig. 4 (c) and (d). The 2,845-mm (112-in.) long specimens appeared to be experiencing closer to a punching shear failure than a flexure failure of the joint. The 1,422-mm (56-in.) long specimens were all experiencing a clear flexure failure within the capacity of the available load frame used in the experimental investigation. A flexure failure was desired for this testing, so the 1,422-mm (56-in.) length was chosen for the construction of the experimental specimens.

F. D. Chitty, C. J. Freeman, and D. B. Garber, "Joint Design Optimization for Accelerated Construction of Slab Beam Bridges," *Journal of Bridge Engineering*, vol. 25, no. 7. p. 04020029-14, 2020

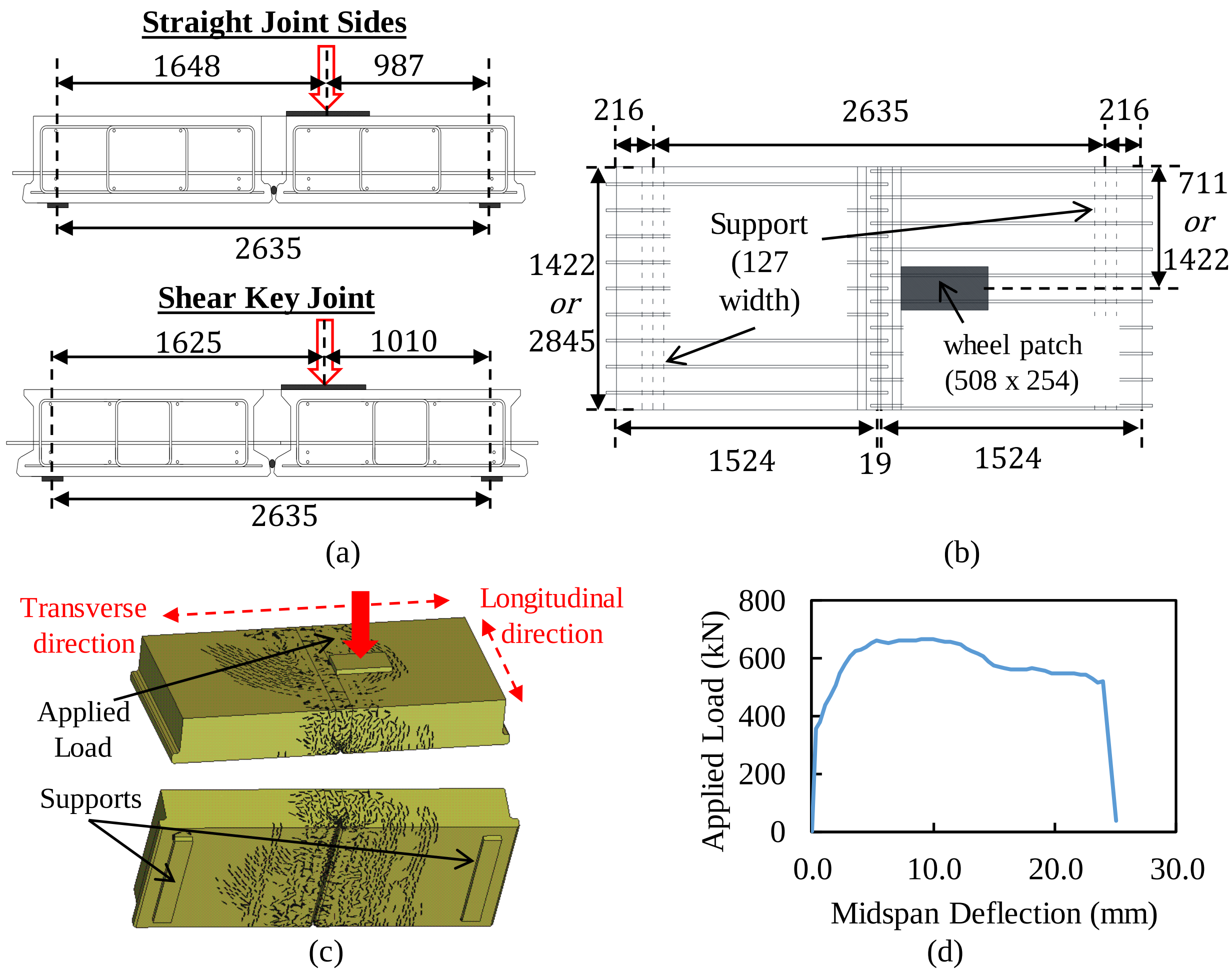

Fig. 4: *Transverse capacity evaluation: (a) applied load relative to joint and supports, (b) top view of wheel patch location, (c) 18F1 top and bottom expected cracking pattern before failure (others similar), and (d) 18F1 estimated load-deflection response (others similar). (length units: mm, 1 mm = 0.0394 in)*

The principal stress that developed in the joints under different load conditions was also investigated through the FEA. The maximum principal stress for the four joint shapes in the 305-mm (12-in.) deep specimens are shown in Fig. 5. There was a concentrated stress that developed at service loading at the bottom of the UHPC joint immediately above the bottom ledge. This concentrated stress was due to a perfect bond being assumed between the top of the ledge and the

UHPC joint. As a result, the top of the ledge was not specified as an exposed aggregate finish for the beams constructed for the experimental investigation. Additionally, cracking and concentrated stresses were observed in the top lip of joint A1, shown in Fig. 5 (b). Joint A2 was developed using FEA to modify the joint to decrease these stress concentrations in the top lip of the joint. The FEA results were validated through the experimental investigation.

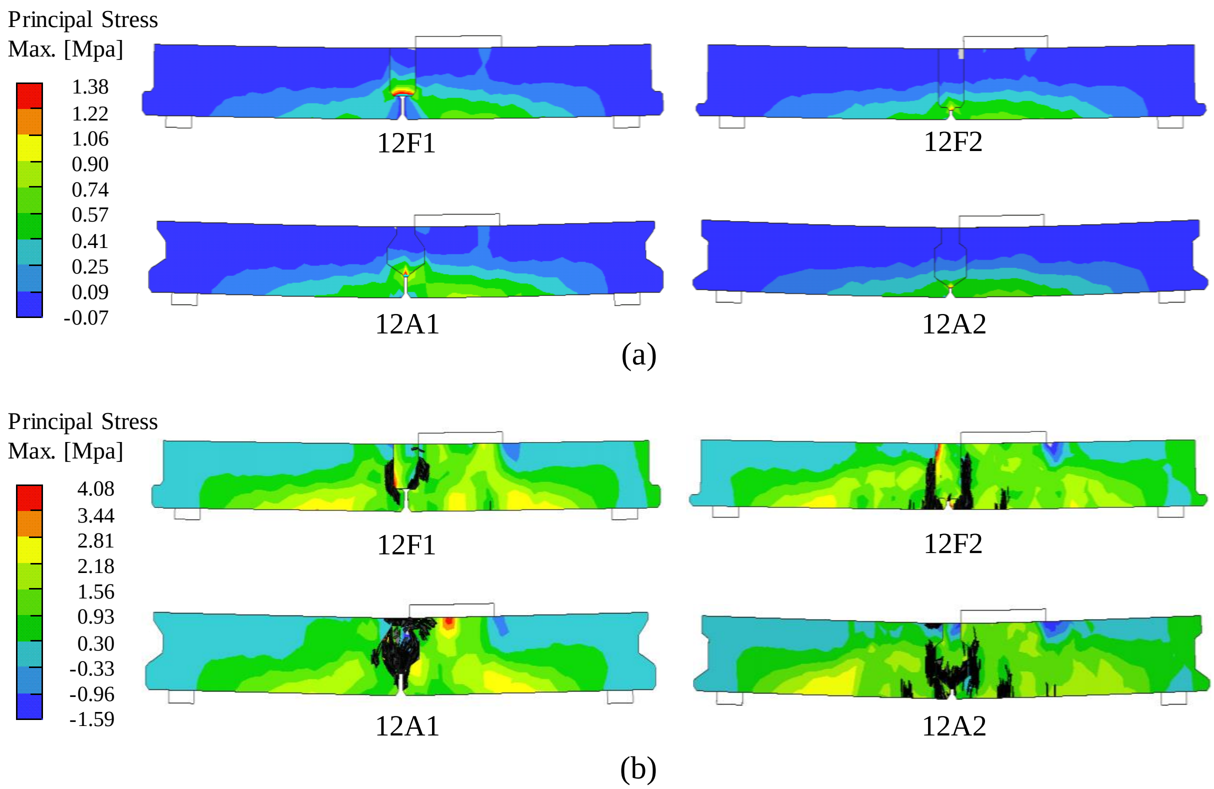

Fig. 5: *Maximum principal stress at the load point in 305-mm (12-inch) deep specimens from FEA at (a) service load of 35.6 kN (8 kips) and (b) ultimate load (load dependent on joint type) with cracking in the plane shown in black (1 MPa = 0.15 ksi)*

EXPERIMENTAL INVESTIGATION

Specimen Design and Material Properties

Sixteen (16) prestressed slab-beam sections, 1,422-mm (56-in.) long by 1,524-mm (60-in.) wide, were built by a local precaster to construct the joint systems using two beams each, shown in Fig. 2. Six of these beams were 457-mm (18-in.) deep (18F1, 18F2, and 18A1 pairs). The other 10 were precast at 305-mm (12-in.) deep (12F1, 12F2, 12A1, 12A2, and FSB pairs). The FSB section was precast at 305-mm (12-in.) deep and then a 152-mm (6-in.) deep CIP deck was cast on top with the joint giving the overall tested section a depth of 457 mm (18 in.). The thicknesses for all the specimens were summarized in Fig. 3. The reinforcement details for each modified joint beam was based on the original FSB design (FDOT, 2016b). Two joint tests were conducted for each pair of precast beams, designated by the last number in the specimen name (e.g., 18F2-1 is the first test on the 18F2 set of specimens).

The precast concrete mix specified for all the beam specimens was FDOT Concrete Class VI with a minimum compressive strength at 28 days of 58.6 MPa (8,500 psi) and maximum water/cement ratio of 0.37 kg/kg (lb/lb). The required concrete mix for the CIP deck in the original FSB joint was FDOT Class II (bridge deck) with a minimum compressive strength at 28 days of 31 MPa (4,500 psi) and maximum water/cement ratio of 0.44 kg/kg (lb/lb). The UHPC mix used for the joint connections was specified to be Ductal® JS1000, which is a proprietary UHPC mixture commonly used for field-cast closure pours for prefabricated bridge element connections. The UHPC mix ingredients, dosages, and mixing procedure were all provided by the manufacturer. The specified and assumed concrete compression strength for the precast section and joint material are shown in Fig. 3.

Table 3: *Material properties for experimental specimens*

Specimen	Section f'_c (MPa)		Joint f'_c (MPa)		Thickness of section (mm)	Joint Preparation
	Specified	*Measured*	*Specified*	*Measured*		
FSB-1	58.6	85.5	27.6	44.8	457.2*	Sandblasted[1]
FSB-2	58.6	87.6	27.6	9.7	457.2*	Sandblasted[1]
18A1-1	58.6	77.9	144.8	164.1	457.2	Sandblasted[1,2]
18A1-2	58.6	75.8	144.8	160.6	457.2	Sandblasted[1,3]
18F1-1	58.6	82.0	144.8	169.6	457.2	Sandblasted[1,2]
18F1-2	58.6	80.7	144.8	165.5	457.2	Sandblasted[1,3]
18F2-1	58.6	82.0	144.8	175.8	457.2	Sandblasted[1,2]
18F2-2	58.6	84.1	144.8	171.7	457.2	Sandblasted[1,3]
12A1-1	58.6	86.2	144.8	160.0	304.8	Sandblasted[1,2]
12A1-2	58.6	95.1	144.8	178.6	304.8	Sandblasted[1,3]
12F1-1	58.6	85.5	144.8	160.0	304.8	Sandblasted[1,2]
12F1-2	58.6	86.2	144.8	187.5	304.8	Sandblasted[1,3]
12F2-1	58.6	81.4	144.8	164.8	304.8	Sandblasted[1,2]
12F2-2	58.6	86.2	144.8	168.9	304.8	Sandblasted[1,3]
12A2-1	58.6	77.2	144.8	166.9	304.8	Paste Retarder[3,4]
12A2-2	58.6	84.1	144.8	175.8	304.8	Paste Retarder[3,4]

Note: f'_c = *concrete compressive strength at 28 days; *thickness of section includes 152.4 mm CIP deck;* [1]*sandblasting resulted in an exposed aggregate finish with less than 1.6 mm roughness;* [2]*joint UHPC was mixed with improper admixtures;* [3]*joint UHPC was mixed with proper admixtures;* [4]*Use of paste retarder resulted in an exposed aggregate finish with 3.2 mm roughness; 1 in. = 25.4 mm; 1 ksi = 6.9 MPa.*

The precast beam fabrication, beam delivery to the FDOT Structures Research Center (SRC), UHPC joint casting, and FSB deck fabrication are shown in Fig. 6. Three sizes of Grade 60 mild steel reinforcement were used to build all the precast specimens: #10 (#3), #13 (#4), and #16 (#5) reinforcement. Ten fully bonded, pre-tensioned, 15-mm (0.6-in.) diameter Grade 270 strands were used in the precast sections with a small amount of prestressing (103.4 MPa [50 ksi]), as shown in Fig. 3. The strands were needed to support the mild reinforcement in the beam section, but likely did not play a role in the transverse capacity of the joint strength.

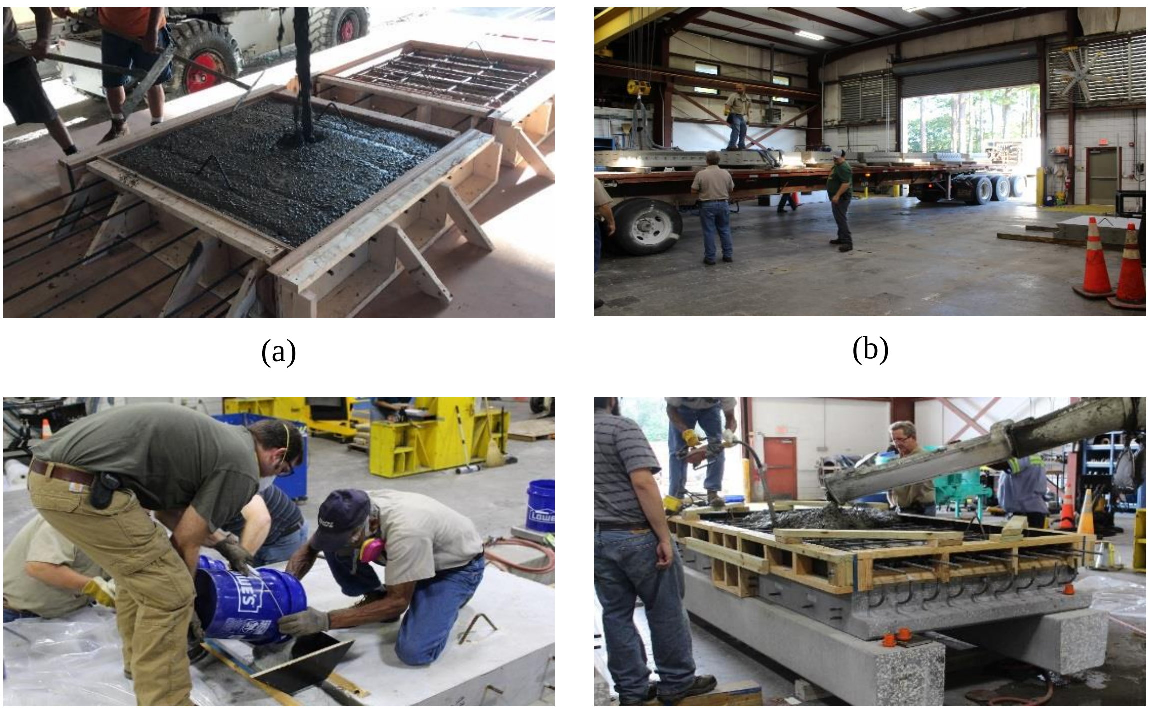

(a) (b) (c) (d)

Fig. 6: *Construction of joint specimens: (a) precast specimen concrete pour, (b) delivery of slab-beam specimens to FDOT SRC, (c) casting of field-cast UHPC, and (d) FSB deck casting.*

Test Setup and Loading Protocol

The supports and testing frame used for the experimental program are shown in Fig. 7. The test setup consisted of two main supports parallel to the joint and holding the specimens in a simply-supported configuration with a vertical clearance of 1,118 mm (44 in.) from the ground to the bottom of the specimen; this allowed to monitor displacements and cracks underneath the joint for ease. Each support was grouted to the strong floor to ensure levelness and avoid undesired movement or rotations. The simply-supported specimens were loaded by a hydraulic jack with a 2,046.2-kN (460 kip) static and fatigue capacity and a variable stroke length of 254 mm (10 in.). The load application point was a steel plate with a 508-mm by 254-mm (20-in. by 10-in.) surface area and 51-mm (2-in.) thickness with a bottom neoprene bearing pad of the same size. The load area is similar to the wheel patch of an AASHTO HS-20 truck (AASHTO, 2014).

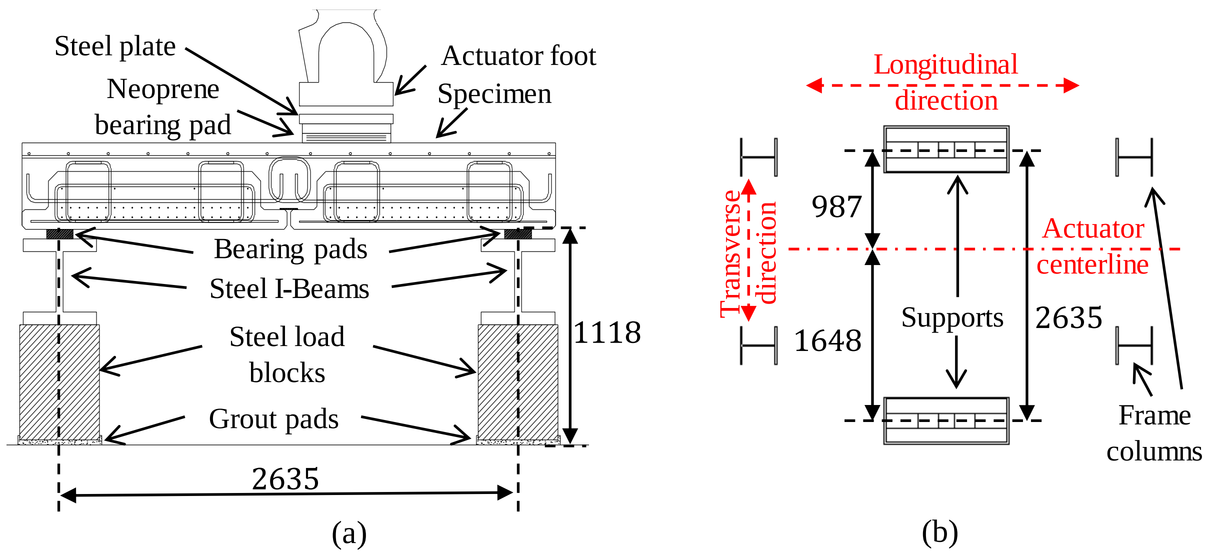

Fig. 7. *Testing frame layout: (a) supports elevation and specimen layout and (b) supports plan layout (actuator centerline parallel to longitudinal joint). (units: mm, 1 mm = 0.0394 in)*

Specimens were tested to determine their ultimate strength and fatigue performance. Strength testing consisted of the application of a monotonic load at an approximate rate of 0.9 kN/s (0.2 kips/s). Loading was typically applied in 44.5-kN (10-kip) increments until 65 percent of the expected ultimate capacity. The specimen being tested was inspected for cracks, cracks marked, and pictures taken in between each load step until 65 percent was reached. The specimen was then gradually loaded until failure.

Two joint tests were performed on each pair of beams as both beam sides were built with the specified joint geometry. After the first test was performed, the connected specimens were cut on one side of the joint region (if the beams did not break apart during test). Then, the beams were rotated so that the unaffected joints were aligned, the joint was cast, and a second test performed. All the specimens were evaluated in the strength test twice, except for 12F1, 12A1, and 12A2. These three specimens were tested once for strength alone and once for fatigue and strength.

The loading protocol for fatigue testing was designed to assess the fatigue performance of the joint on a low-volume, 4-lane urban collector bridge over a 100-year service life, to see if this fatigue loading would lead to cracking, debonding between the UHPC and precast system, or other degradation of the joint performance. This first stage of fatigue loading consisted of 1.1 million cycles of load between 8.9 kN and 56.2 kN (2 kip and 12.64 kip) at 2 Hz. The upper limit value was obtained using a single HS-20-wheel load amplified to include a dynamic load allowance of 33 percent. This dynamic load allowance should have been 15 percent for fatigue limit states, but the results with the 33 percent dynamic load allowance are conservative.

The second stage of fatigue loading was used to evaluate the effect of cycling from below to above the cracking load on crack and damage growth, debonding of joint reinforcement, and overall degradation of the system performance. The fatigue load range was selected based on the static test results. The lower fatigue load was selected approximately 10 percent less than the cracking load measured from the static tests. The load range was selected such that the stress range in the joint reinforcement was 137.9 MPa (20 ksi), a stress range recommended by Helgason et al. (Helgason, Hanson, Somes, Corley, & Hognestad, 1976) to avoid fatigue of the reinforcement itself since this was not the purpose of this fatigue testing. The stress range was determined based on strain measurements in the joint reinforcement during the static testing. Using this stress range, a load range of 84.5 kN to 133.4 kN (19 kip to 30 kip) was selected for these specimens. The scheduling of the laboratory testing allowed for a total of 2 million cycles for all the fatigue stages for each specimen, so 900,000 cycles at this post-cracking load range were applied to each of the three specimens tested in fatigue.

The ultimate strength of the specimens after the fatigue loading were then determined through a static loading protocol similar to that described earlier. This post-fatigue static testing was performed to see if fatigue testing had any negative influence on the ultimate strength of the joint.

Instrumentation

Four types of sensors were used to measure the response of the joint specimens: unidirectional concrete surface strain gauges oriented perpendicular to the joint, unidirectional rebar strain gauges installed on each joint rebar, linear crack opening transducers across the bottom joint between beams, and laser displacement transducers to measure the vertical deflections at different locations of the specimen. The laser displacement transducers were placed at three locations along the joint on the top of the specimen. The hydraulic jack had a built-in load cell capable of measuring the load being applied to the joint sample.

EXPERIMENTAL RESULTS AND DISCUSSION

A summary of the measured flexural strengths found through the experimental testing is shown in Fig. 8 alongside the estimated flexural strength from FEA and stress block calculations per AASHTO § 5.6.3.2.3 (AASHTO, 2014). Results from the first and second test on each joint are shown with a different shading used to highlight when the second test was performed after fatigue testing of a joint. The load versus deflection response for all of the experimental specimens are shown in Fig. 9 (a) for the 457-mm (18-in.) specimens and Fig. 9 (b) for the 305-mm (12-in.)

specimens. The load-deflection curve for the FSB specimen is also shown as a comparison point for the 457-mm (18-in.) deep UHPC joints.

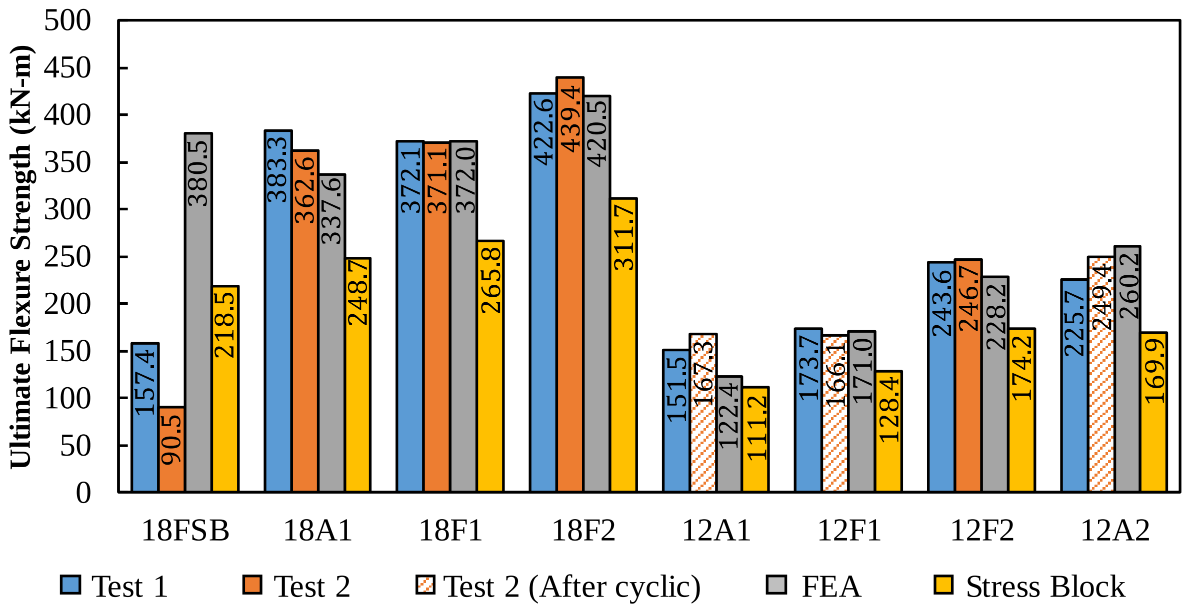

Fig. 8: *Ultimate flexural strength comparison. (1 kN-m = 0.738 k-ft)*

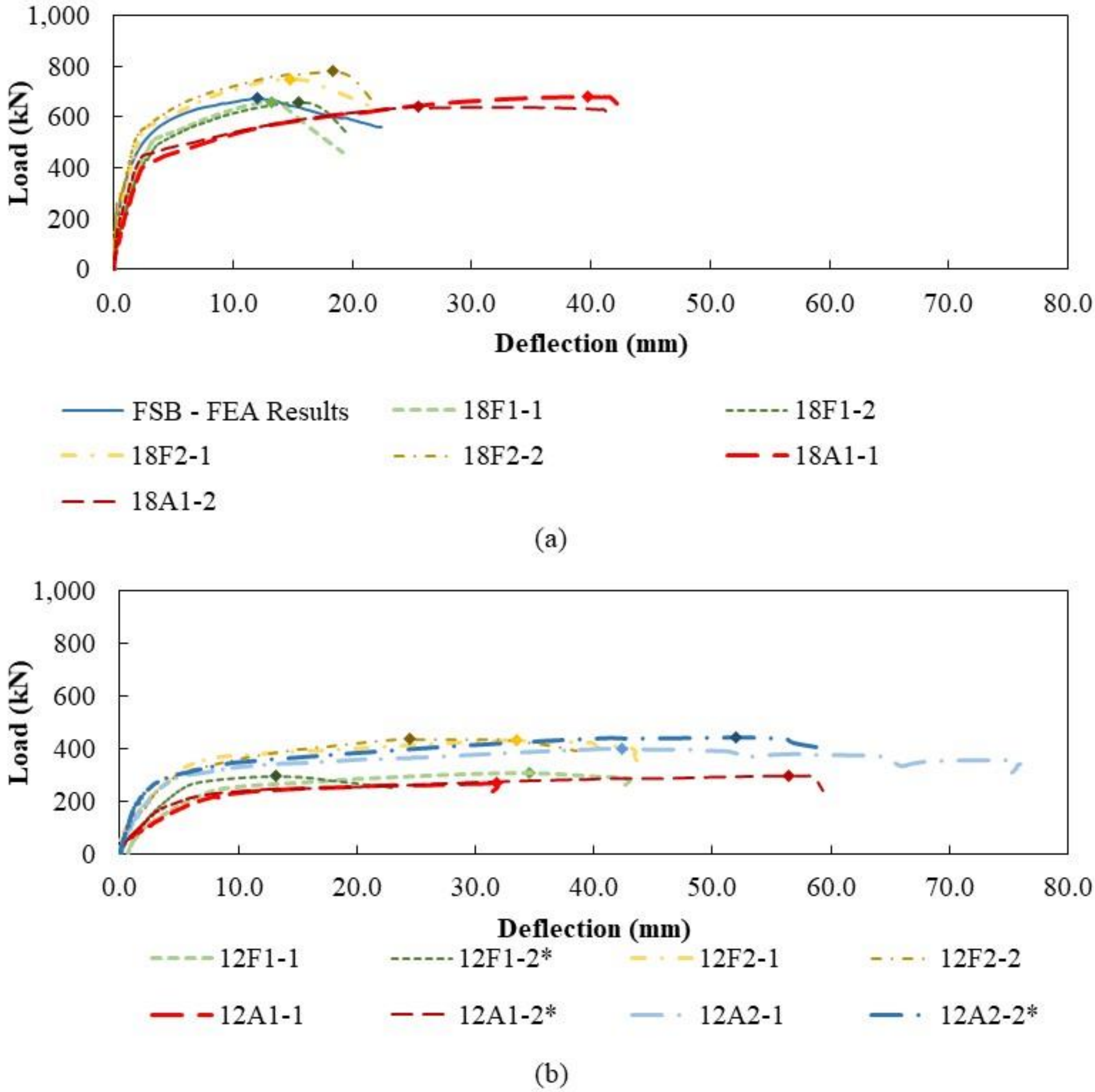

Fig. 9: *Load versus deflection responses with maximum loads for (a) 457-mm (18-inch) deep and (b) 305-mm (12-inch) deep specimens; *Monolithic response after fatigue testing completed*

Performance of Numerical Modeling

There was an overall good agreement between the numerical results and the experimental results other than for the FSB specimens, see Fig. 8. The predicted ultimate flexural strength in the 457-mm (18-in.) specimens was in good agreement with the experimental response (less than 10 percent difference): 18F1 with 372 kN-m (3,293 k-in) predicted versus 371.5 kN-m (3,288 k-in) average from tests, 18F2 with 420.5 kN-m (3,722 k-in) versus 431 kN-m (3,815 k-in) average from tests, and 18A1 with 337.6 kN-m (2,988 k-in) versus 373 kN-m (3,301 k-in) average from tests. There was also good agreement of the predicted and tested experimental ultimate flexural strength for the 305-mm (12-inch) specimens: 12A1 with 122.5 kN-m (1,084 k-in) versus 159.6 kN-m (1,413 k-in) average from tests, 12F1 with 171 kN-m (1,514 k-in) versus 169.9 kN-m (1,504 k-in) average from tests, 12F2 with 228.2 kN-m (2,020 k-in) versus 245.1 kN-m (2,169 k-in) average from tests, and 12A2 with 260.2 kN-m (2,303 k-in) versus 237.6 kN-m (2,103 k-in) average from tests. There was a significant difference between the estimated and measured response for the FSB specimens, due to a different failure mechanism occurring in the tested FSB specimens than predicted by the FEA. The FEA results for the FSB specimens were used as the comparison point for the developed UHPC joints due to the overall good agreement between the FEA and experimental results for the other specimens. An estimated strength was also determined using the rectangular stress block approach for calculating nominal flexural strength; this estimated strength was less than the measured strength for all test specimens other than the FSB specimens.

Performance of Current FSB Joint Detail

Both FSB control specimen tests failed due to a development failure of the joint reinforcement before yielding of the joint reinforcement occurred, as shown in Fig. 10 (a). The specimens had the same slope as the FEA model estimate until a crack developed at the location of one hook, which was the beginning of the development failure. The specimens then continued to maintain load as the specimen continued to deflect resulting from the hook pulling out of the joint. The original FSB design guidelines (FDOT, 2016a) specify #16 (#5) joint reinforcement with a 90-degree hook and typical 64-mm (2.5-in.) bend diameter, as shown in Fig. 10 (b). The hooked joint reinforcement from adjacent beams is spliced together with hoop bars and straight bars extending the length of the joint placed between the hook and the hoop. This detail was designed to ensure proper force transfer between adjacent beams. The actual bend diameter of this joint reinforcement was larger than specified, as shown in Fig. 10 (c). This larger bend diameter resulted in the joint reinforcement not being able to develop, which led to a lower transverse flexural capacity than expected. The larger bend diameter resulted in the constructed hook having lower bearing stresses in the bend region and less length for stresses on the back of the tail of the hook to prevent the tail from kicking out; both of these factors would have contributed to the development failure of the hook. Additionally, the longitudinal reinforcement, placed inside the bend radius of the joint reinforcement to improve the splice behavior, bent during testing making it less effective at aiding with the splice connection. Additional joint reinforcement was added to the joint for FSB-2 to improve the splice behavior, but a much lower concrete strength was received for this joint than was specified, which further contributed to a lower failure load.

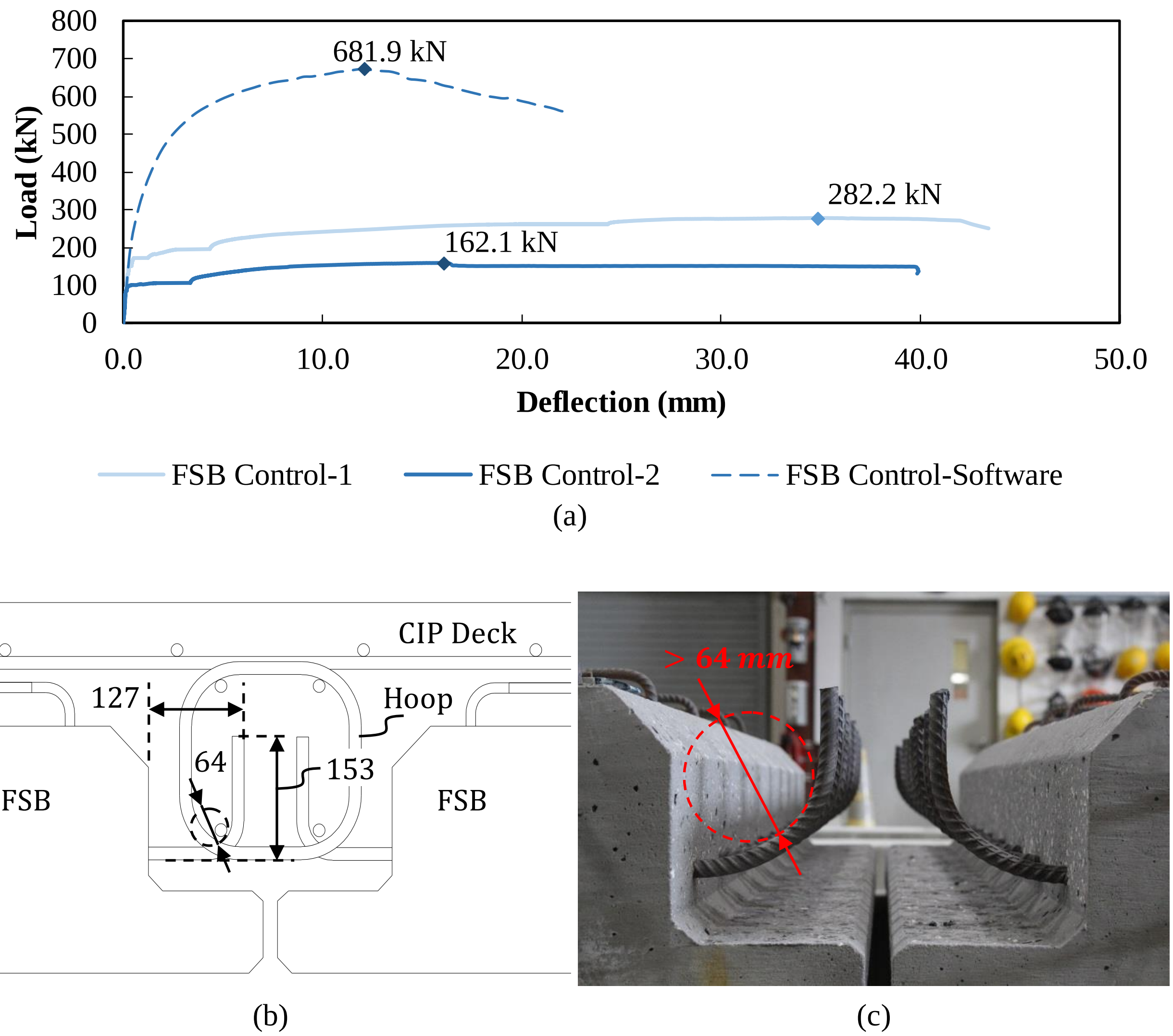

Fig. 10: *FSB joint performance: (a) load versus deflection response (b) specified joint detail with 64-mm bend diameter for hooks and (c) actual joint reinforcement with larger than 64-mm bend diameter for hooks. (length units: mm, 1 mm = 0.0394 in)*

These test results highlight the importance of having the proper bend diameter, reinforcement detail and joint concrete strength for satisfactory performance of the joint. Although the proper bend diameter was not achieved in the test specimens for this research, there are no issues reported right now in the field with already deployed FSB systems. This may be due to a combination of the properly constructed detail exhibiting satisfactory behavior and the actual joint not experiencing the same level of load that was tested.

Performance of Developed Joint Details

When looking at the 457-mm (18-in.) deep specimens, the UHPC joints performed similar to or better than the predicted response for the FSB control specimen. The 18F2 joint had the highest capacity, with about a 10-percent higher capacity that the FSB control and other joints. This higher capacity was a result of an increased lever arm of the joint reinforcement, which translated to enhanced transverse flexural capacity. Though the increased lever arm came at the cost of constructability, as the 51-mm (2-in.) bottom lip with no reinforcement extending into it can be easily broken off during fabrication and shipping. The other 457-mm (18-in.) deep specimens (18F1 and 18A1) had similar capacities to the FSB control specimen as their lever arms only varied by about 10 mm (0.4 in.). The 18A1 joint had an increased ultimate deflection and deflection at ultimate load; 18A1 had the largest ultimate deflection and deflection at ultimate load of all the investigated UHPC joint details due to increased joint rebar embedment length.

The 305-mm (12-in.) deep specimens were tested to compare the flexural performance of the joint in the thinnest standard slab beam section that is standardized by FDOT. Because the current standard is a 305-mm (12-in.) deep precast section with a 153-mm (6-in.) thick CIP deck, no control comparison was possible for the 305-mm (12-in.) deep members. The lever arm of the joint reinforcement had a more pronounced impact on the flexural strength of these members: 12F2 and 12A2 had the largest lever arm for the joint reinforcement and had the highest strength. The available embedment and splice length impacted the ductility of the section: 12A2 had a larger splice length and an embedment length equal to or larger than the other joints and had the highest ductility. Finally, the ultimate strength of the joints was not negatively impacted by the applied

F. D. Chitty, C. J. Freeman, and D. B. Garber, "Joint Design Optimization for Accelerated Construction of Slab Beam Bridges," *Journal of Bridge Engineering*, vol. 25, no. 7. p. 04020029-14, 2020

fatigue loading. 12A1, 12F1, and 12A2 all had similar ultimate strengths after fatigue loading (test 2) compared to their strengths without fatigue loading first (test 1).

There were two primary failure modes observed in the joint specimens:

1. **Failure due to lack of embedment or splice length**: Three different types of development failures were observed in the joint reinforcement, shown in Fig. 11 (a), (b), and (c), due to a lack of embedment or splice length provided. In FSB-1 a failure occurred when crack developed at the location of the hook in the joint reinforcement, see Fig. 11 (a). The reinforcement in 18F1-1, 12F1-2, and 12F2-2 experienced a development failure of the joint reinforcement when there was some combination of a splitting crack developing at the location of the reinforcement and a cone developed around the joint reinforcement along the length of the joint. 12F1-2 had a splitting crack visible on the outside of the joint at the level of the joint reinforcement, see Fig. 11 (b). For 18F1-1 and 18F2-2, the UHPC remained bonded to some of the joint reinforcement, but a cone of UHPC around the reinforcement pulled away with some of the reinforcement from the joint causing a development failure, see Fig. 11 (c) and (d); this type of development failure typically occurs when there is sufficient bond between the reinforcement and concrete but insufficient embedment or splice length. Many of these development failures started with cracking along the interface between the precast section and UHPC joint.

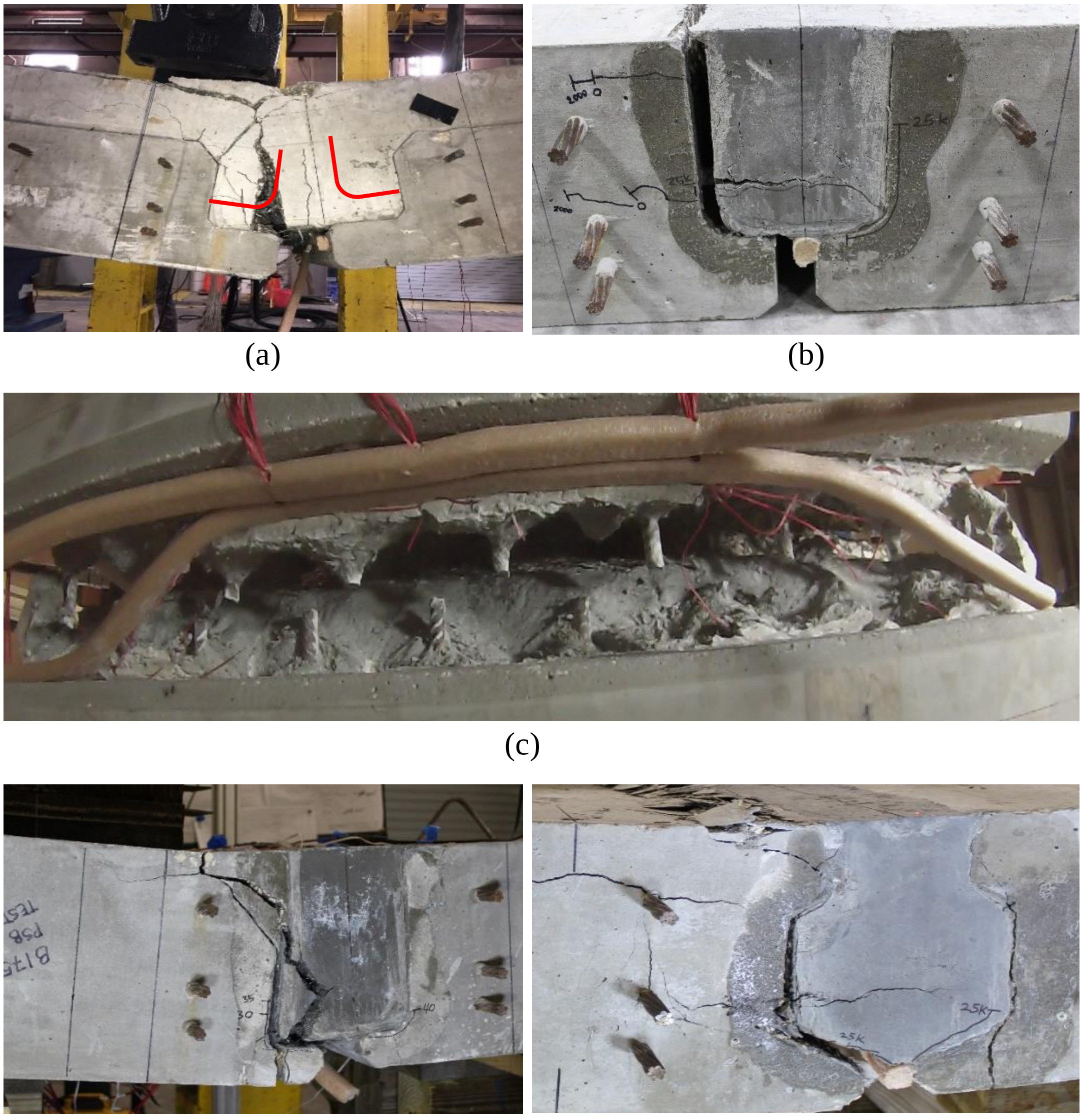

(a) (b) (c) (d) (e)

Fig. 11: *Failure mechanism observed during testing: (a) pullout of hooked reinforcement in FSB-1 (hooked joint reinforcement shown), (b) pullout of straight joint reinforcement caused by splitting crack in 12F1-1 (splitting crack shown after unloading), (c) pullout of straight joint reinforcement in 18F1-1 (bottom view shown), (d) pullout of straight joint reinforcement with conical failure in 12F2-2, and (e) crushing of concrete in top of section in 12A2-1.*

2. **Crushing of concrete at top of section**: Crushing of concrete along the top of the joint and fracture of joint reinforcement was the predominant failure in the specimens with a diamond shaped joints (18A1, 12A1, and 12A2), similar to Fig. 11 (e). These specimens had a larger deflection at ultimate load and ultimate deflection, as highlighted in Fig. 9. Fracture of the joint reinforcement in these specimens was observed in these specimens when the load was removed, and they were removed from the test frame.

There were constructability issues and early cracking observed in the specimens with 51-mm (2-in.) thick bottom lips (12F2 and 18F2). The precaster commented that it was difficult to cast this specimen at only a 1,422-mm (56-in.) length and it would be very difficult for them to cast a full-length beam, as the lip can easily break off when the formwork is being removed. The bottom lip on one of the specimens (12F2) was damaged during shipping and placement of the beams; a repair was done on this specimen before casting of the UHPC joint. Additionally, cracking extended through the bottom lip in all these specimens, as shown in Fig. 11 (c).

Interface Surface Finish and Bond to UHPC

The experimental testing also revealed the importance of surface finish and the workability of UHPC to achieve sufficient bond between the precast concrete and UHPC in the joint. Past research has shown that an exposed aggregate finish with a 6.3-mm (0.25-in.) magnitude surface roughness provides good texture for adequate bond between the precast element and the fresh UHPC (Graybeal, 2014a). This finish is traditionally achieved by painting a paste retarder on formwork prior to casting and then using a pressure washer to remove the soft cement paste within 24 hours of casting.

Fourteen (14) of the 16 beams were cast at the same time. Heavy sandblasting was used for the specimens 305-mm and 457-mm (12-in. and 18-in.) deep with F1, F2, and A1 joints, to achieve the specified 6.3-mm (0.25-in.) magnitude exposed aggregate finish that has been recommended by previous researchers (Graybeal, 2014a). The finish that was achieved for these specimens, shown in Fig. 12 (a), was less than 1.6 mm (0.0625 in.), not the specified 6.3-mm (0.25-in.) magnitude finish. Additionally, incorrect admixtures were initially sent with the UHPC that provided only a short working time and limited flowability of the UHPC for the first tests on these joint specimens. These two factors led to debonding between the precast section and UHPC joint in all these tests, as shown in Fig. 12 (b) and (c). The proper admixtures for sufficient working time and flowability were obtained for casting of the joints for all the second tests, but debonding still occurred in these tests, which was likely a result of having a smoother joint surface finish than specified.

The recommended procedure for achieving the exposed aggregate finish was used for the last two specimens that were cast (12A2). A set-retarding admixture was painted on the side forms prior to casting. The forms were removed one day after casting, and the surface was pressure washed using constant 24.1 MPa (3,500 psi) water pressure at a controlled distance of application. A 3.2-mm (0.125-in.) magnitude exposed aggregate finish was achieved using the recommended procedure, shown in Fig. 12 (d). Although the finish was not the recommended 6.3-mm (0.25-in.) magnitude, it still offered improved bond compared to the sandblasted finish, as shown in Fig. 12 (e).

F. D. Chitty, C. J. Freeman, and D. B. Garber, "Joint Design Optimization for Accelerated Construction of Slab Beam Bridges," *Journal of Bridge Engineering*, vol. 25, no. 7. p. 04020029-14, 2020

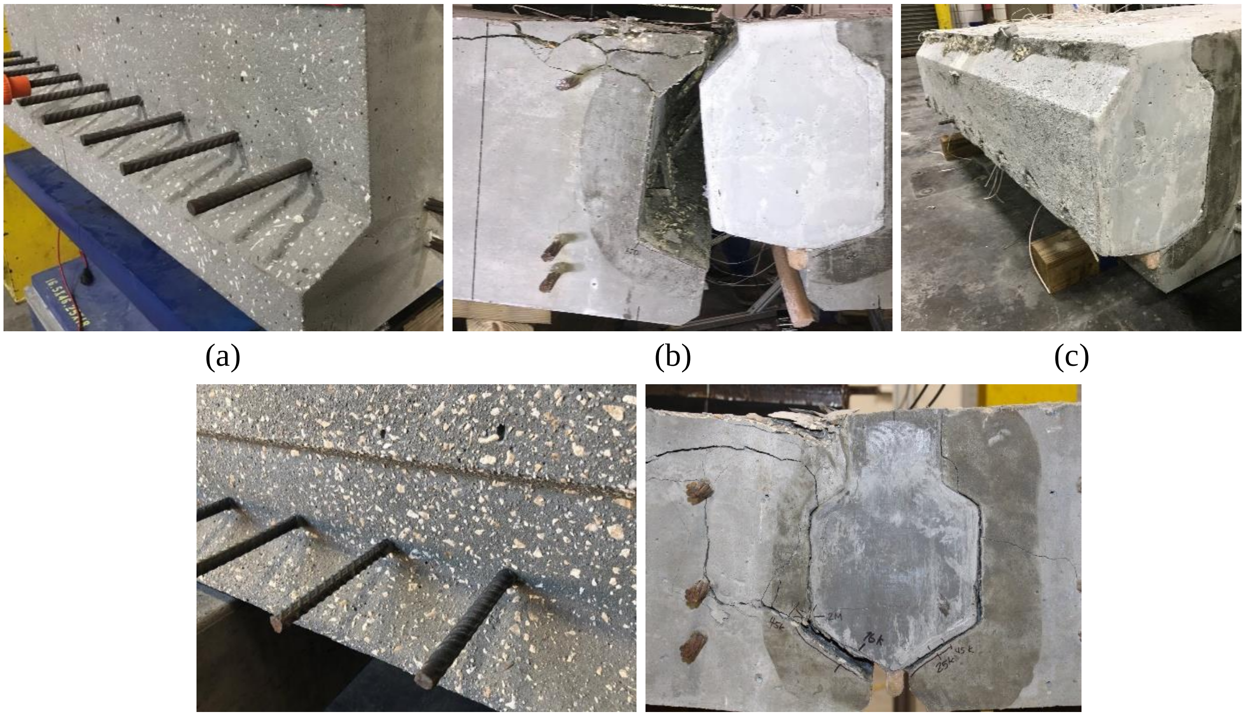

(a) (b) (c)

(d) (e)

Fig. 12: *Impact of joint surface finish on performance: (a) surface finish obtained using heavy sandblasting, (b) debonding during testing of 18A1-1 (occurred in majority of these specimens with sandblasted finish), (c) failure plane of 18A1-1 after specimen removed from test setup, (d) surface finish obtained using paste retarder on forms for 12A2-2, (e) failure of 12A2-2.*

Even though the precast joint surface finish did not seem to play a role in the ultimate capacity of the connection under monotonic load, it is thought to be a critical factor in the long-term service life of the joint. Insufficient bond may lead to early separation at the interface, which can expose the protruding steel to early pollution penetration like carbonation and/or chlorides in harsh marine environments. This can impact the transverse capacity and may lead to the slab beam superstructure no longer behaving as a solid unit.

Fatigue Performance of Joint Specimens

Fatigue testing was conducted on three of the 305-mm (12-in.) deep joint specimens: 12F1-2, 12A1-2, and 12A2-2. The normalized absolute stiffness for all three fatigue specimens is shown in Fig. 13 (a) through (c), respectively. The stiffness was calculated every thousandth cycle by dividing the difference between the upper and lower applied load by the corresponding difference between the upper and lower deflection. The normalized stiffness was found by dividing this calculated stiffness for every thousandth cycle by the stiffness of the first cycle, as described by Garber (Garber, Gallardo, Deschenes, & Bayrak, 2015). Cracking of these specimens or other degradation in overall behavior caused by fatigue loading would cause a change in the normalized stiffness. For 12A1-2 and 12A2-2, the change in normalized stiffness can be seen between the before and after cracking fatigue phases. 12F1-2 was accidentally cracked prior to fatigue loading generating two transverse cracks extending from the joint region to the precast section, seen at both joint end sides (at the level of joint reinforcement); this accidental crack pattern was similar to the pattern seen on 12A1-2 and 12A2-2 after concluding the after-cracking phase. Although the accidental load was not measured, the magnitude was larger than the specimen cracking load, thought to be between 178 and 222 kN (40 and 50 kips). The accidental load is the reason why there was no change in the normalized stiffness between the before and after cracking fatigue phases, and there was no further crack growth or decay of behavior during the cycle applications. Overall, there was no noticeable drop in the stiffness in any of the three joints that would indicate cracking in the joint during the before-cracking phase or decay in the joint strength capacity during the after-cracking phase.

F. D. Chitty, C. J. Freeman, and D. B. Garber, "Joint Design Optimization for Accelerated Construction of Slab Beam Bridges," *Journal of Bridge Engineering*, vol. 25, no. 7. p. 04020029-14, 2020

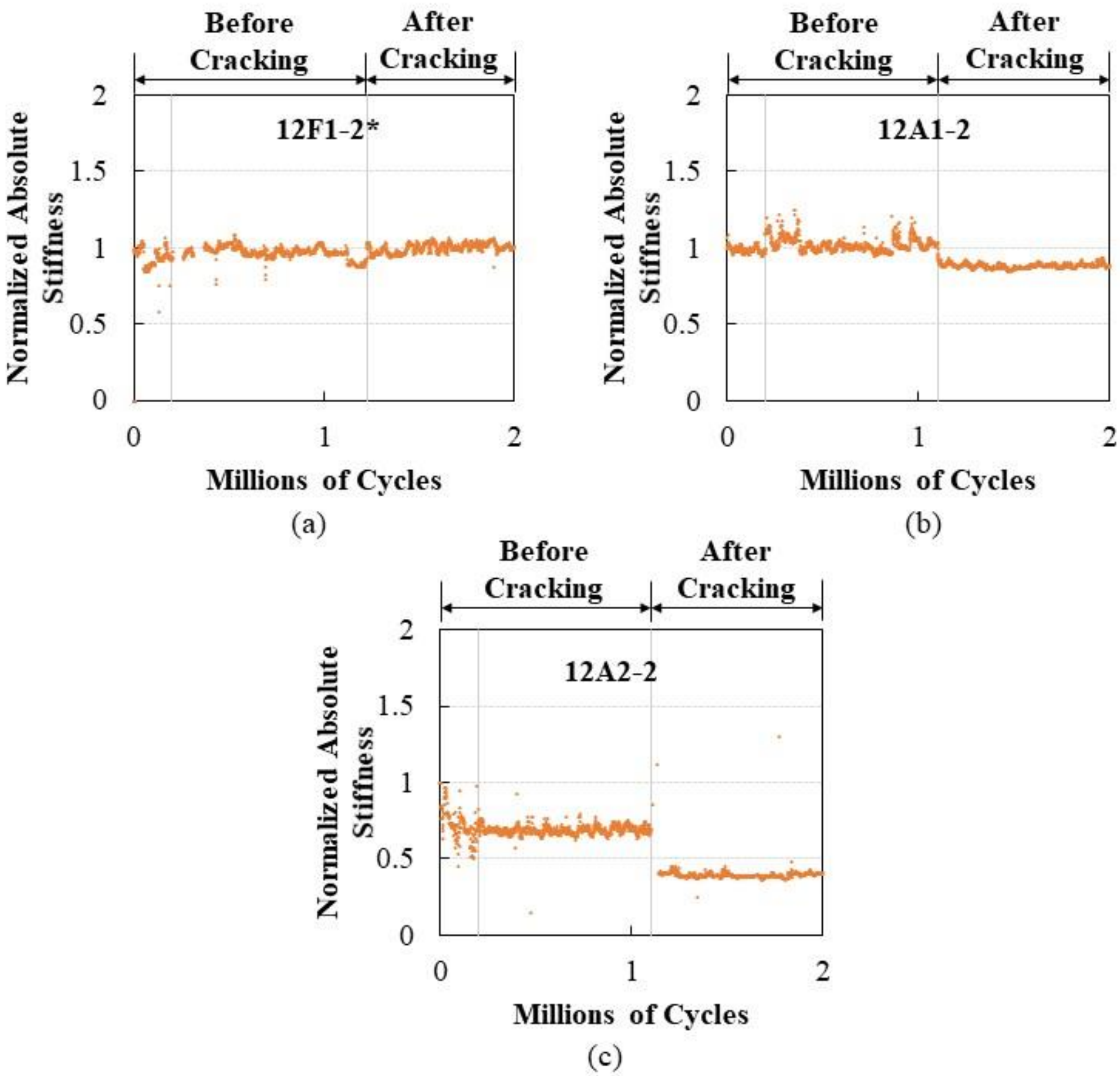

Fig. 13: *Normalized absolute stiffness every thousandth cycle of system for joints (a) 12F1-2, (b) 12A1-2, and (c) 12A2-2. *Cracked specimen due to accidental load.*

Also, as previously mentioned, the ultimate strength of each joint was tested following the fatigue testing. The ultimate strengths were comparable for specimens tested with and without prior fatigue testing: the ultimate strength of 12F1-2 decreased by about four percent after fatigue testing, and the ultimate strength of 12A1-2 and 12A2-2 both increased by about 10 percent. These measured ultimate strengths with and without fatigue testing have similar variability to the two tests conducted without fatigue testing (18A1, 18F1, 18F2, and 12F2), as shown in Fig. 8.

CONCLUSIONS

Several conclusions can be made based on the construction and experimental results of the joint tests:

- The control FSB joint (FSB-1 and FSB-2) did not perform as expected due to a larger bend diameter (FSB-1) and due to the compressive strength of the deck concrete being much lower than specified (FSB-2). These issues caused development failure of the joint reinforcement prior to yield.
- All 457-mm (18-in.) deep UHPC joints performed similar to or better than the predicted response of the FSB section using FEA (assuming no development failure occurred).
- Joint 18A1 (with a shear key and increased embedment length of the joint reinforcement) had the largest deflection at ultimate load and largest ultimate deflection of the 457-mm (18-in.) deep joints with a comparable ultimate strength.
- Joint 12A2 (with a shear key and increased embedment and splice length of the joint reinforcement) was the best performing joint of those tested. Although a 457-mm (18-in.) version was not tested experimentally, the benefits of this joint over 12A1 (with a shear key and shorter splice length of the joint reinforcement than 12A2) will likely translate well to the 457-mm (18-in.) version.
- A 51-mm (2-in.) thick bottom lip with no reinforcement extending into it presents challenges with constructability. A thicker bottom lip with reinforcement is recommended for similar slab beam members.

- Using heavy sandblasting on the precast beams with SCC resulted in an exposed aggregate finish of less than 1.6 mm (0.0625-in.). Using a paste retarding agent on similar beams provided a 3.2-mm (0.125-in.) magnitude exposed finish, which resulted in improved bond for the two specimens tested (12A2-1 and 12A2-2).
- The pre-cracking fatigue loading stage did not cause cracking or show any signs of deterioration in performance for 12A1-2 and 12A2-2. The after-cracking fatigue loading stage did not cause degradation of the overall behavior for 12A1-2, 12A2-2, and 12F1-2. Fatigue loading had little effect on the ultimate strength of joints 12A1-2, 12A2-2 and 12F1-2.

Based on the results of this testing, joint 12A2 (with a modified shear key shape and longer non-contact lap splice) appears to have the best performance and constructability. Future testing is planned on full-scale beams to determine actual joint demands and behavior, provide a comparison with the demand on the tested small-scale specimens, and develop complete design recommendations.

NOTATIONS

d_b = diameter of joint reinforcement

E = modulus of elasticity

f'_c = compressive strength of concrete

f_t = tensile strength of concrete

f_y = yield strength of steel reinforcement

G_F = fracture energy

l_d = required development or embedment length

l_s = required lap splice length

DATA AVAILABILITY STATEMENT

Some or all data, models, or code generated or used during the study are available from the corresponding author by request.

- Videos from testing
- Select data from testing and FEA models

ACKNOWLEDGEMENTS

The research presented in this project was supported by the Florida Department of Transportation (FDOT). The authors would like to thank FDOT for their financial support and the team of engineers and staff at the Structures Research Center for their assistance in constructing and testing the specimens. The opinions, findings and conclusions expressed in this publication are those of the author(s) and not necessarily those of the Florida Department of Transportation or the U.S. Department of Transportation.

REFERENCES

Aaleti, S., & Sritharan, S. (2014). Design of Ultrahigh-Performance Concrete Waffle Deck for Accelerated Bridge Construction. *Transportation Research Record: Journal of the Transportation Research Board, 2406*, 12–22. https://doi.org/10.3141/2406-02

American Association of State Highway and Transportation Officials (AASHTO). (2014). *AASHTO LRFD Bridge Design Specification, Customary U.S. Units, 7th Edition*. Washington, D. C.

American Society of Civil Engineers (ASCE). (2017). *2017 Infrastructure Report Card*.

Bell, C. M., French, C. E., & Shield, C. K. (2006). *Application of precast decks and other elements to bridge structures* (No. MN/RC-2006-37; p. 271). Minneapolis, MN: University of Minnesota.

Cervenka, J., & Papanikolaou, V. (2008). Three Dimensional Combined Fracture-Plastic Material Model for Concrete. *International Journal of Plasticity*, *24*, 2192–2220. https://doi.org/10.1016/j.ijplas.2008.01.004

Cervenka, V., Jendele, L., & Cervenka, J. (2016). *ATENA Program Documentation - Theory* (p. 330). Cervenka Consulting.

Federal Highway Administration (FHWA). (2015). MnDOT/FHWA Precast Slab System Workshop Summary Report. Retrieved from https://www.fhwa.dot.gov/bridge/prefab/slab.cfm

Florida Department of Transportation (FDOT). (2013). *SURVEY: FDOT Superstructure Types for Short and Medium Spans*.

Florida Department of Transportation (FDOT). (2016a). Developmental Design Standards. *Index No. D20450 Series Florida Slab Beam*. Retrieved from http://www.dot.state.fl.us/rddesign/DS/Dev/IDDS/IDDS-D20450.pdf

Florida Department of Transportation (FDOT). (2016b). Instructions for Developmental Design Standards. *Index D20450 Series Florida Slab Beam*. Retrieved from http://www.dot.state.fl.us/rddesign/DS/Dev/IDDS/IDDS-D20450.pdf

French, C., Shield, C., Klaseus, D., Smith, M., Eriksson, W., Ma, Z., … Chapman, C. E. (2011). *Cast-in-Place Concrete Connections for Precast Deck Systems (Web-Only Document 173)*. Retrieved from National Academies of Sciences, Engineering, and Medicine website: https://doi.org/10.17226/17643

Garber, D., Gallardo, J., Deschenes, D., & Bayrak, O. (2015). Experimental Investigation of Prestress Losses in Full-Scale Bridge Girders. *ACI Structural Journal*, *112*(5), 12.

Goldsberry, B. (2015). *Florida Slab Beam (FSB) - Development and Implementation*. Presented at the Design Training Expo. Retrieved from http://www.dot.state.fl.us/officeofdesign/Training/DesignExpo/2015/presentations/FSBDevelopmentandImplementation-BenGoldsberry.pdf

Graybeal, B. A. (2006). *Material property characterization of ultra-high performance concrete* (No. No. FHWA-HRT-06-103). Federal Highway Administration.

Graybeal, B. A. (2010). *Behavior of Ultra-High Performance Concrete Connections between Precast Bridge Deck Elements*. Presented at the 2010 Concrete Bridge Conference: Achieving Safe, Smart & Sustainable Bridges.

Graybeal, B. A. (2014a). *Design and construction of field-cast UHPC Connections* (No. FHWA-HRT-14-084; p. 36). Federal Highway Administration.

Graybeal, B. A. (2014b). Ultra-high-performance concrete connections for precast concrete bridge decks. *PCI Journal*.

Haber, Z., De la Varga, I., Graybeal, B., Nakashoji, B., & El-Helou, R. (2018). *Properties and Behavior of UHPC-Class Materials* (No. FHWA-HRT-18-036; p. 153). Federal Highway Administration.

Halverson, M., French, C., & Shield, C. (2012). *Full-Depth Precast Concrete Bridge Deck System: Phase II* (Final Report No. MN/RC 2012-30; p. 204). Minneapolis, MN: University of Minnesota.

Helgason, T., Hanson, J. M., Somes, N. F., Corley, W. G., & Hognestad, E. (1976). Fatigue Strength of High-Yield Reinforcing Bars. *NCHRP Report*, (164).

Hordijk, D. (1991). *Local Approach to Fatigue of Concrete* (Dissertation). Technische Universiteit Delft, The Netherlands.

F. D. Chitty, C. J. Freeman, and D. B. Garber, "Joint Design Optimization for Accelerated Construction of Slab Beam Bridges," *Journal of Bridge Engineering*, vol. 25, no. 7. p. 04020029-14, 2020

Menkulasi, F., Cousins, T., & Wollmann, R. (2018). *Implementation of a Precast Inverted T-Beam System in Virginia: Part II: Analytic and Field Investigation* (Final Report No. FHWA/VTRC 19-R2; p. 76). Blacksburg, VA: Virginia Polytechnic Institute and State University.

Menkulasi, F., Mercer, M., Wollmann, C., & Cousins, T. (2012). Accelerating Bridge Construction Using the Precast Inverted T-Beam Concept. *Precast/Prestressed Concrete Institute (PCI)*.

Nolan, S., Freeman, C., Kelley, A., & Rossini, M. (2018, October). *Advancing Small Bridges (Florida Down Under)*. Presented at the 5th International fib Congress, Melbourne, AU.

Russell, H. G., & Graybeal, B. A. (2013). *Ultra-High Performance Concrete: A State-of-the-Art Report for the Bridge Community* (No. FHWA-HRT-13-060; p. 171). Federal Highway Administration.

Smith, M., Eriksson, W., Shield, C., & French, C. (2008). *Monitoring and Analysis of Mn/DOT Precast Composite Slab Span System (PCSSS)* (No. MN/RC 2008-41; p. 219). Minneapolis, MN: University of Minnesota.

Texas Department of Transportation (TxDOT). (2018). *Prestressed Concrete Decked Slab Beam Standards* (No. table14e). Retrieved from https://www.dot.state.tx.us/insdtdot/orgchart/cmd/cserve/standard/bridge-e.htm

Yuan, J., & Graybeal, B. (2014). *Bond Behavior of Reinforcing Steel in Ultra-High Performance Concrete* (Final Report No. FHWA-HRT-14-090; p. 78). McLean, VA: Office of Infrastucture Research & Development.

Yuan, J., Graybeal, B., & Zmetra, K. (2018). *Adjacent Box Beam Connections: Performance and Optimization* (No. FHWA-HRT-17-093; p. 129). Federal Highway Administration.